doi:10.1016/j.jmb.2011.08.044 J. Mol. Biol. (2011) 413, 615–627

Contents lists available at www.sciencedirect.com

Journal of Molecular Biology

journal homepage: http://ees.elsevier.com.jmb

Crystallographic Analysis of the Primary Photochemical Reaction of Squid Rhodopsin

Midori Murakami [1] and Tsutomu Kouyama [1,2*]

[1]*Department of Physics, Graduate School of Science, Nagoya University, Nagoya 464-8602, Japan*
[2]*RIKEN Harima Institute/SPring-8, 1-1-1, Kouto, Mikazuki, Sayo, Hyogo 679-5148, Japan*

Received 9 May 2011;
received in revised form
19 August 2011;
accepted 23 August 2011
Available online
31 August 2011

Edited by R. Huber

Keywords:
visual transduction;
G-protein-coupled receptor;
retinal;
seven-transmembrane protein;
X-ray damage

Visual signal transduction is initiated by the photoisomerization of 11-*cis* retinal upon rhodopsin ligation. Unlike vertebrate rhodopsin, which interacts with Gt-type G-protein to stimulate the cyclic GMP signaling pathway, invertebrate rhodopsin interacts with Gq-type G-protein to stimulate a signaling pathway that is based on inositol 1,4,5-triphosphate. Since the inositol 1,4,5-triphosphate signaling pathway is utilized by mammalian nonvisual pigments and a large number of G-protein-coupled receptors, it is important to elucidate how the activation mechanism of invertebrate rhodopsin differs from that of vertebrate rhodopsin. Previous crystallographic studies of squid and bovine rhodopsins have shown that there is a profound difference in the structures of the retinal-binding pockets of these photoreceptors. Here, we report the crystal structures of all-*trans* bathorhodopsin (Batho; the first photoreaction intermediate) and the artificial 9-*cis* isorhodopsin (Iso) of squid rhodopsin. Upon the formation of Batho, the central moiety of the retinal was observed to move largely towards the cytoplasmic side, while the Schiff base and the ionone ring underwent limited movements (i.e., the all-*trans* retinal in Batho took on a right-handed screwed configuration). Conversely, the 9-*cis* retinal in Iso took on a planar configuration. Our results suggest that the light energy absorbed by squid rhodopsin is mostly converted into the distortion energy of the retinal polyene chain and surrounding residues.

Introduction

Rhodopsin, the primary photoreceptor molecule in the visual signaling cascade, contains 11-*cis* retinal that is attached through the protonated Schiff base to a lysine residue in the seventh transmembrane helix. Upon absorption of light, the retinal chromophore isomerizes to the all-trans configuration, producing the first photoreaction intermediate, bathorhodopsin (Batho). It is widely believed that Batho stores distortion energy in the retinal-binding pocket, which is utilized as a driving force in the formation of subsequent intermediates (lumirhodopsin and metarhodopsin) and eventually activates the conjugated G-protein.[1–4] Previous studies of bovine rhodopsin by NMR, Raman spectroscopy, and Fourier transform infrared spectroscopy have suggested that the retinal chromophore in Batho takes on a largely distorted all-trans configuration.[5–9] Time-resolved spectroscopy has shown that photoisomerization from the 11-*cis* retinal to the all-*trans* retinal takes place very rapidly ($\tau \sim 500$ fs)[10,11] and at a high quantum efficiency ($\phi = 0.67$).[12,13] However, when the retinylidene chromophore with the protonated Schiff base is excited in solution, isomerization from the 11-cis configuration to the all-trans configuration occurs at a much slower rate ($\tau \sim 10$ ns) and at a lower quantum efficiency ($\phi \sim 0.3$).[14] These results suggest that the protein environment has a

*Corresponding author. Department of Physics, Graduate School of Science, Nagoya University, Nagoya 464-8602, Japan. E-mail address: kouyama@bio.phys.nagoya-u.ac.jp.

Abbreviations used: Batho, bathorhodopsin; Iso, isorhodopsin; Rhod, unphotolysed rhodopsin.

profound influence on the excited-state dynamics of the retinal protein.

Recent crystallographic studies of squid and bovine rhodopsins have shown that although the overall architecture of transmembrane helices is conserved in these rhodopsins, there is a profound difference in the structures of the retinal-binding pockets.[15–17] First, the β-ionone ring of retinal in squid rhodopsin is surrounded by several aromatic residues, whereas bovine rhodopsin possesses a glutamate in the vicinity of the ionone ring. Second, retinal in squid rhodopsin associates with the backbone of helix III over three helical turns, while this tight contact is prevented in bovine rhodopsin, which has a polar residue (Thr118) in the region of contact. As a consequence, the retinal polyene chain is more distorted in bovine rhodopsin than in squid rhodopsin. A significant difference in the structure near the retinal Schiff base is also observed. In squid rhodopsin, the hydrogen-bonding partner of the Schiff base is either the side-chain carbonyl of Asn87 or the OH group of Tyr111. These residues are replaced by glycine (Gly89) and glutamate (Glu113), respectively, in bovine rhodopsin.

The photochemical properties of squid rhodopsin are different largely from those of bovine rhodopsin, reflecting the structural differences between them. For example, bovine rhodopsin is hydrolyzed to free retinal and apoprotein (opsin) after photoactivation, whereas a long-lived photoactivated state (metarhodopsin) of squid rhodopsin is thermally stable and reverts to the dark state upon absorption of a second photon.[1] The structure of bovine rhodopsin suggests that the binding affinity of retinal, which is kept high owing to the salt bridge between the Schiff base and its counterion (Glu113), is reduced when this salt bridge is broken in the photoactivated state.[18] Conversely, such a reduction is unlikely to occur in squid rhodopsin, where the Schiff base interacts indirectly with the putative counterion Glu180 via the side chain of Asn185.

Since there is a difference in the charge distribution around retinal for squid and bovine rhodopsins, it may be argued that energy storage in the primary photoreaction of squid rhodopsin is considerably different from that in the primary photoreaction of bovine rhodopsin. Structural analysis of Batho has been previously performed for bovine rhodopsin.[19] It has been suggested that interconversion between unphotolysed rhodopsin (Rhod) and Batho is accompanied by a limited configurational change in the central part of retinal without detectable changes in surrounding residues. Recent theoretical studies of visual pigments have predicted that the local environment of retinal assists in the efficient isomerization of retinal.[20] Against this background, structural analysis of the primary photoreaction of squid rhodopsin would lead to a better understanding of the influence of the protein environment on chromophore isomerization and on the activation process of rhodopsin.

It has been shown that excitation of Batho induces a reaction back to the initial state (Rhod), as well as formation of isorhodopsin (Iso), an artificial state containing 9-*cis* retinal.[4,21] As a consequence, the photoequilibrium state of rhodopsin at a cryogenic temperature was determined by interconversions among the three states (i.e., 11-*cis* Rhod, all-*trans* Batho, and 9-*cis* Iso). For the structural analysis of the primary photoreaction of squid rhodopsin, it is important to take into account the following issues: (1) high Iso content in a photoequilibrium state that is established by illumination at a cryogenic temperature; and (2) possible effects of X-ray radiation damage on the crystal structure. When squid rhodopsin was illuminated with yellow light at a cryogenic temperature, the population of Iso was much higher than those of Rhod and Batho.[4,22,23] In this study, the structure of Iso was first determined using diffraction data collected under an illumination condition where Iso became the major isomeric component. Subsequently, structural information on Batho was extracted by analyzing a difference electron density map that was deduced from two diffraction data sets collected under different illumination conditions. During these structural investigations, however, we found that the retinal chromophore in squid rhodopsin was modified by a very low dose of X-rays ($\sim 10^{14}$ photons/mm^2), as previously observed for bacteriorhodopsin.[24] Since the structural change associated with the primary photoreaction is small, it is crucially important to quantify how much X-ray radiation damage affects the structure of squid rhodopsin. By employing an experimental procedure where possible effects of X-ray damages were minimized, we were able to determine the true conformational change associated with the primary photoreaction and the structural difference between Rhod and Iso.

Results

Isomeric composition in a photoequilibrium state at 100 K

It has been shown that the photo steady state of squid rhodopsin at a cryogenic temperature (77–135 K) is described by light-initiated interconversions among the three isomeric states: Rhod(11-cis) ↔ Batho (all-trans) ↔ Iso(9-cis).[4] To elucidate the excited-state dynamics of squid rhodopsin in a frozen crystal, we recorded the absorption spectra before and after illumination with visible light at various wavelengths (Fig. 1a). At 100 K, squid rhodopsin in an unilluminated crystal exhibited maximum absorption at 482 nm, which is redshifted by 2 nm from that observed at 277 K. When the frozen crystal was

illuminated with blue light at 473 nm, a redshifted species (i.e., Batho absorbing maximally at 535 nm) and a blueshifted species (i.e., Iso absorbing maximally at 468 nm) were generated. When this crystal was subsequently illuminated with yellow light at 560 nm, the absorption peak shifted to 468 nm. This shift was accounted for by the accumulation of Iso, whose absorption coefficient at 560 nm is much smaller than that of the other isomeric states (Fig. 1c). A similar but less significant blueshift was induced when the crystal that was preilluminated with blue light was illuminated with red light at ≥ 620 nm.

In principle, isomeric composition after illumination at λ_{ex} [$c_{rhod}(\lambda_{ex})$, $c_{batho}(\lambda_{ex})$, and $c_{iso}(\lambda_{ex})$] can be evaluated from the absorption spectrum of the illuminated crystal $A(\lambda;\lambda_{ex})$ if the absorption spectra (ε_{rhod}, ε_{batho}, and ε_{iso}) of the individual isomeric components are given: $A(\lambda;\lambda_{ex}) = c_{rhod}(\lambda_{ex})\varepsilon_{rhod}(\lambda) + c_{batho}(\lambda_{ex})\varepsilon_{batho}(\lambda) + c_{iso}(\lambda_{ex})\varepsilon_{iso}(\lambda)$. For determination of ε_{batho} and ε_{iso}, $A(\lambda;\lambda_{ex})$ values recorded after illumination at various wavelengths (λ_{ex}) were analyzed using the approximations described as follows:

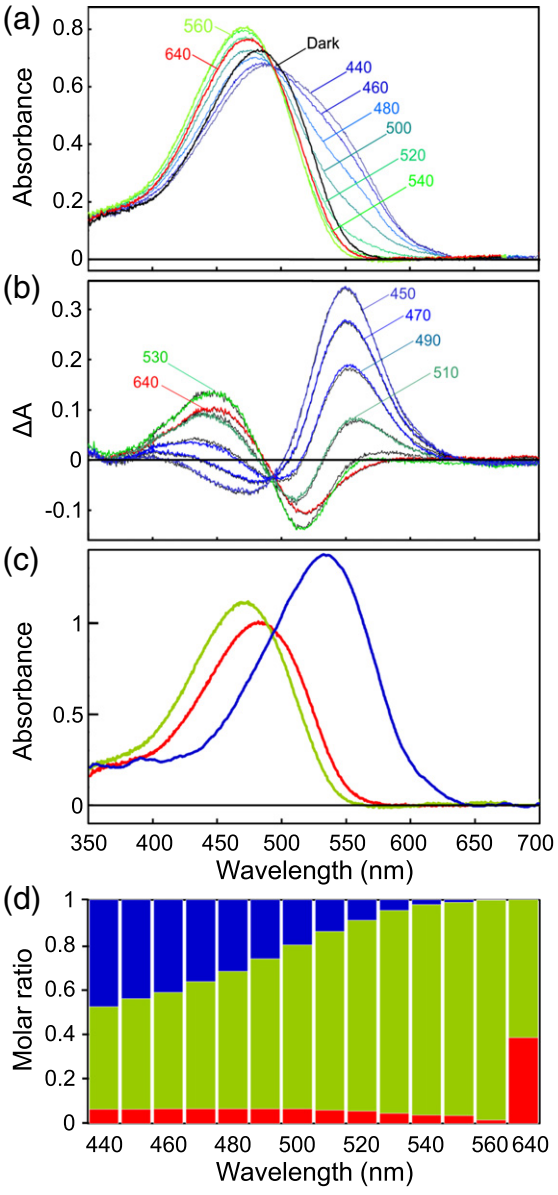

1. A photoequilibrium state is established under illumination with light at a short wavelength ($\lambda_{ex} \leq 560$ nm), where, the isomeric composition is given by the following equations:

$$c_{batho} / c_{rhod} = \phi_{batho-rhod}\varepsilon_{batho}(\lambda_{ex}) / \phi_{rhod-batho}\varepsilon_{rhod}(\lambda_{ex})$$

$$c_{batho} / c_{iso} = \phi_{batho-iso}\varepsilon_{batho}(\lambda_{ex}) / \phi_{iso-batho}\varepsilon_{iso}(\lambda_{ex})$$

where $\phi_{rhod-batho}$, $\phi_{batho-rhod}$, $\phi_{batho-iso}$, and $\phi_{iso-batho}$ are the quantum efficiencies of Rhod-to-Batho, Batho-to-Rhod, Batho-to-Iso, and Iso-to-Batho photoconversions.

2. Only Batho is excited when the crystal is illuminated with red light ($\lambda_{ex} \geq 620$ nm), that is, the isomeric composition after red-light illumination [c_{rhod}(red) and c_{iso}(red)] is given by the following equations:

$$c_{rhod}(\text{red}) = c_{rhod}(\text{blue}) + \gamma_{rhod}c_{batho}(\text{blue})$$

$$c_{iso}(\text{red}) = c_{iso}(\text{blue}) + (1 - \gamma_{rhod})c_{batho}(\text{blue})$$

where c_{rhod}(blue), c_{batho}(blue), and c_{iso}(blue) represent the isomeric composition before red-light illumination, and $\gamma_{rhod} = \phi_{batho-rhod}/(\phi_{batho-iso} + \phi_{batho-rhod})$.

When the excited-state dynamics of squid rhodopsin was assumed to be described by the

Fig. 1. Light-initiated interconversions among the three isomers (Rhod, Batho, and Iso) in a frozen crystal at 100 K. (a) Absorption spectra observed before (black line) and after (colored lines) illumination at various wavelengths. Numerals represent the wavelength of actinic light (emission from a 150-W halogen–tungsten lamp was passed through a bandpass interference filter with a 10-nm bandwidth and focused on the frozen crystal). (b) Difference spectra obtained by subtracting the absorption spectrum of the unilluminated crystal from those recorded after illumination at various wavelengths (colored lines). The black lines represent difference spectra that were derived from the calculated absorption spectra of the three isomers after taking into account the dependence of the isomeric composition on the wavelength of actinic light. (c) Calculated absorption spectra of Batho (blue line) and Iso (green line) compared with the absorption spectrum of Rhod (red line). (d) The isomeric composition in the illuminated crystal is plotted against the wavelength of actinic light. Blue, green, and red bars represent the relative contents of Batho, Iso, and Rhod, respectively.

common excited-state model [i.e., $\phi_{batho-rhod} = \gamma_{rhod}(1-\phi_{rhod-batho})$ and $\phi_{batho-iso} = (1-\gamma_{rhod})(1-\phi_{iso-batho})$], iterative least-squares analysis of the spectral data gave the following quantum efficiencies: $\phi_{batho-rhod} = 0.78$, $\phi_{batho-rhod} = 0.21$, $\phi_{batho-iso} = 0.034$, and $\phi_{iso-batho} = 0.013$. When the common excited-state model was not utilized, slightly different values ($\phi_{batho-rhod} = 0.69$, $\phi_{batho-rhod} = 0.14$, $\phi_{batho-iso} = 0.030$, and $\phi_{iso-batho} = 0.011$) were obtained on the assumption that the quantum efficiency $\phi_{rhod-batho}$ was similar to that ($\phi_{rhod-batho} = 0.69$) reported for octopus rhodopsin. It should be noted that although absolute quantum efficiencies are difficult to determine accurately, the calculated absorption spectra of Batho and Iso are less sensitive to the assumption about excited-state dynamics. Figure 1c shows the most likely absorption spectra of Batho and Iso. These calculated absorption spectra are similar to those reported by Shichida *et al.*, who investigated the absorption spectra of solubilized squid rhodopsin at 77 K.[22]

Using the calculated absorption spectra of Batho and Iso, we evaluated the contents of Rhod, Batho, and Iso in the illuminated crystal as follows: 6%, 37%, and 57% after blue-light illumination ($\lambda_{ex} = 473$ nm); 2%, 0%, and 98% after yellow-light illumination ($\lambda_{ex} = 560$ nm); and 38%, 0%, and 62% after red-light illumination ($\lambda_{ex} = 635$ nm). The present estimation of the high content of Iso after yellow-light illumination is in good agreement with that (~95%) deduced by an HPLC analysis of the retinal extraction of an illuminated sample of squid rhodopsin.[23]

X-ray-induced absorption changes in the $P6_2$ crystal

To investigate how rapidly squid rhodopsin in the $P6_2$ crystal at 100 K is modified by X-rays, we

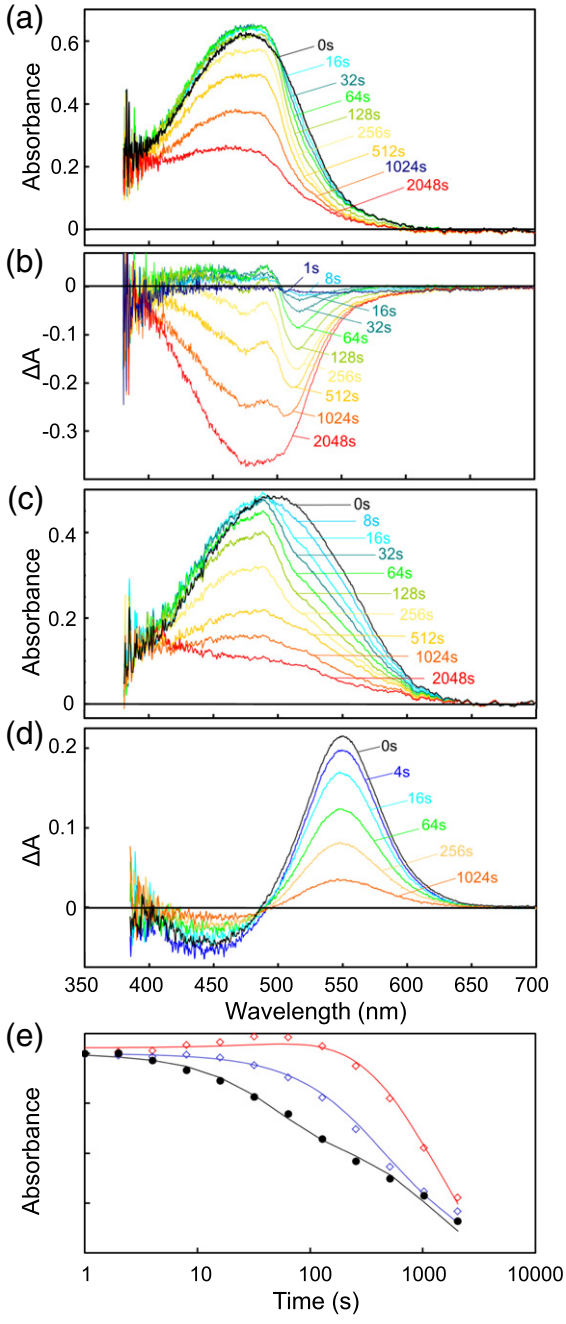

Fig. 2. X-ray-induced absorption changes in the $P6_2$ crystal at 100 K. (a) Absorption spectra observed before (black line) and after (colored lines) a frozen crystal in red light at 635 nm was exposed for various periods to monochromatic X-ray radiation at 1 Å at a flux rate of 4×10^{12} photons/mm^2/s. The numerals in this panel indicate the accumulated exposure time expressed in seconds. (b) Difference spectra derived by subtracting the absorption spectrum of the undamaged crystal (black line in (a)) from those observed after exposure to X-rays for various periods (colored lines in (a)). (c) X-ray-induced absorption changes observed for a frozen crystal that was kept in blue light at 473 nm during X-ray exposure. (d) Red-light-induced absorption changes observed before (black line) and after (colored lines) exposure to X-rays for various periods. Each difference spectrum was obtained in the following manner: (i) a frozen crystal in blue light at 473 nm was exposed to X-rays (4×10^{12} photons/mm^2/s) for a specified period; (ii) blue light was turned off; (iii) two absorption spectra were measured before and after illumination with red light at 635 nm; and (iv) the spectrum before red-light illumination was subtracted from that recorded after red-light illumination. (e) Decay of the content of the photoactive protein during the X-ray exposure of a frozen crystal (black circles), that is, the magnitude (ΔA_{550}) of red-light-induced absorption change in an X-ray damaged crystal (as shown in (c)) is plotted against the accumulated time of X-ray exposure. The experimentally determined decay process of the photoactive protein is fitted by two exponential components with time constants of 50 s and 1200 s (black line). For comparison, the magnitudes of X-ray-induced absorption change at 490 nm observed for a crystal in red light (a) and that observed for a crystal in blue light (c) are shown with red and blue diamonds, respectively.

investigated X-ray-induced absorption changes using an online spectrophotometer. Figure 2a shows the absorption changes observed when a frozen crystal of squid rhodopsin in red light was exposed to synchrotron radiation at a wavelength of 1 Å and at a flux rate of 4×10^{12} photons/mm^2/s. The size of each crystal (<0.1 mm) and the diameter of the measuring light (0.05 mm) used in this measurement were smaller than the beam size of X-ray radiation (0.15 mm × 0.15 mm). With increasing exposure time, absorbance at 520 nm decreased and, instead, an orange species exhibiting absorption peaks at 460 nm and 490 nm appeared. When the exposure time was further increased, the absorption bands in the visible region slowly diminished. This result suggested that the isomers (Rhod and Iso) that accumulated in red light were first modified into orange products, which were then converted into a colorless product at a higher flux of X-rays.

Figure 2c shows X-ray-induced absorption changes observed for a frozen crystal that was kept under illumination with blue light, where approximately 30% of the protein was initially trapped in Batho. In this case, the absorbance at 535 nm (i.e., at the absorption peak of Batho) decreased rapidly, while the absorbance at 420–480 nm decayed slowly after a transient increase. It appeared that, like Rhod or Iso, Batho was first modified into an orange species, which was then converted into a colorless product at a higher flux of X-rays.

These X-ray-induced absorption changes are similar to those previously observed for bacteriorhodopsin.[24] In the case of the neutral purple form of bacteriorhodopsin containing all-*trans* retinal, nearly half of the fraction of the protein was converted into an orange product (a precursor of the retro form of retinal) upon exposure to an X-ray dose of approximately 4×10^{14} photons/mm^2. After an equilibrium state between the intact purple form and its orange X-ray product had ben established (owing to a reverse X-ray reaction), the protein was converted into a colorless product by a much higher dose of X-rays ($\sim10^{16}$ photons/mm^2). From the kinetic analysis of the spectral data shown in Fig. 2a or c, it was suggested that the radiation damage occurring in squid rhodopsin can be described by the same scheme as that proposed for bacteriorhodopsin. To confirm this possibility, we investigated the light-initiated reactions of squid rhodopsin after a frozen crystal in blue light was exposed to X-rays for various periods. In Fig. 2d, each curve represents the difference absorption spectrum that was derived by subtracting the absorption spectrum recorded after blue-light illumination from the absorption spectrum recorded after red-light illumination. It can be seen that although the magnitude of the absorption change induced by red light decreased with increasing time of X-ray exposure, the profile of the associated difference absorption spectrum remained unaltered. This observation suggests that X-ray products of squid rhodopsin were photochemically inactive or silent. It is also suggested that even after a large fraction of the protein had been damaged, the residual fraction of protein underwent normal photoreaction. In Fig. 2e, the amplitude of the red-light-induced absorption change at 550 nm, which is proportional to the content of the undamaged protein, is plotted against the X-ray exposure time (closed circles). Its decay kinetics is described with two time constants. Together with the kinetic analyses of X-ray-induced absorption changes, this result suggested that nearly half of the fraction of the protein was converted into the orange product by an X-ray dose of approximately 2×10^{14} photons/mm^2 and, subsequently, a mixture of the intact form of rhodopsin and the orange X-ray product(s) was converted into a colorless product(s) by an X-ray dose of 5×10^{15} photons/mm^2.

It may be argued that X-ray-initiated modification of retinal chromophore in any member of the rhodopsin superfamily is described by essentially the same scheme. Conversely, it has been reported that X-ray products with different optical properties are generated when different reaction states of bacteriorhodopsin (e.g., the acidic blue form or the yellow M state) are exposed to X-ray doses of 2×10^{14} photons/mm^2 to 4×10^{14} photons/mm^2.[25,26] Therefore, it is natural to suppose that the individual isomers of squid rhodopsin are converted into different X-ray products. In this case, we have to deal with a complicated system in which interconversions among six species take place: (Rhod ⇔ X-rhod) ↔ (Batho ⇔ X-batho) ↔ (Iso ⇔ X-iso), where the symbols ⇔ and ↔ represent interconversion reactions initiated by X-rays and visible light, respectively. On the other hand, kinetic analyses of the spectral data in Fig. 2 suggest that the X-ray-induced interconversions (Rhod ⇔ X-rhod, Batho ⇔ X-batho, and Iso ⇔ X-iso) are reversible processes and that there is no large difference in the reaction efficiencies for the forward and backward reactions. In the following structural analyses, we assumed that the isomeric composition in a frozen crystal exposed to X-rays (and visible light) was determined mainly by the wavelength of visible light.

Structural changes caused by X-ray radiation damages

To elucidate the nature and extent of X-ray radiation damages that proceeded during data collection, we collected two complete diffraction data sets (F_{1st} and F_{2nd}) from a single crystal in red light using a monochromatic X-ray beam at $\lambda=1.0$ Å. When each data set was collected using an X-ray dose of approximately 8×10^{15} photons/mm^2, the $|F_{2nd}|-|F_{1st}|$ difference Fourier map

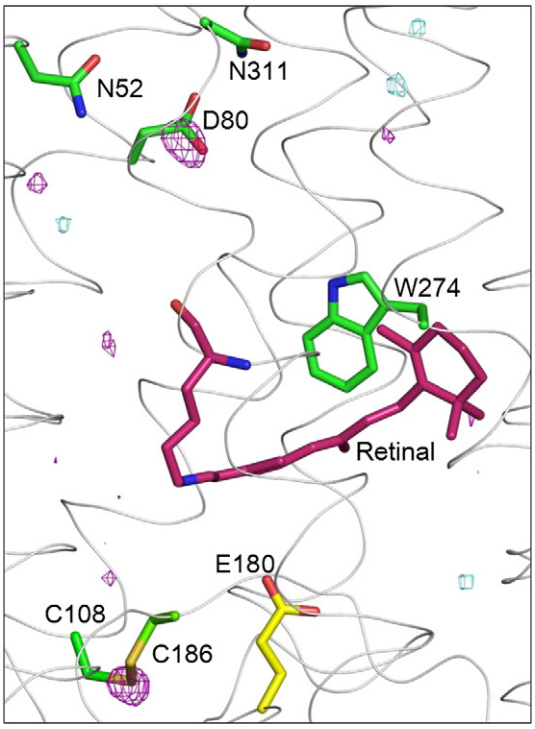

Fig. 3. X-ray-induced structural change in a frozen crystal of squid rhodopsin at 100 K. Two diffraction data sets ($|F_{1st}|$ and $|F_{2nd}|$) from a frozen crystal were serially collected using an X-ray dose of approximately 8×10^{15} photons/mm^2 per data set. The $|F_{2nd}|-|F_{1st}|$ difference electron density map (blue, positive density; purple, negative density) is contoured at 3σ and overlaid on the structural model of Rhod.

exhibited negative peaks at the side chain of Asp80 and at the disulfide bond between Cys108 and Cys186 (Fig. 3). These peaks were not clearly seen when diffraction data were collected using a lower X-ray flux. It is likely that breakage of the disulfide bond between Cys108 and Cys186, which is located in the vicinity of the Schiff base, correlates with the production of a colorless X-ray product. With respect to the loss of electron density at Asp80, it has been reported that negatively charged carboxyl groups are liable to radiolysis.[27] Hence, it is possible that, unlike bovine rhodopsin, Asp80 is deprotonated in squid rhodopsin.

Although the difference map shown in Fig. 3 has no significant peak around retinal, this does not necessarily mean that retinal remained unaffected during data collection. In fact, it is expected from the X-ray-induced absorption changes that modification of the protein into the orange product(s) took place at an early stage of data collection (i.e., exposure to an X-ray dose of approximately 2×10^{14} photons/mm^2 corresponds to the collection of several oscillation images). Unfortunately, we have not yet succeeded in obtaining clear information about retinal configuration in the orange X-ray products (X-rhod, X-batho, or X-iso). This implies that what we can discuss at present is the average structure of an undamaged isomer and its X-ray product. In the following structural analysis, we tentatively assumed that the shape of retinal in any isomeric state did not significantly change upon X-ray absorption. The possible effects of this assumption on our interpretation of the structural data will be discussed later.

Structural changes induced by visible light

If no X-ray damages took place, the following difference electron density maps would be calculated: (1) $\Delta\rho(\text{Red–Blue})\equiv\rho(\text{Red})-\rho(\text{Blue})=0.32\rho_{\text{rhod}}-0.37\rho_{\text{batho}}+0.05\rho_{\text{iso}}$; (2) $\Delta\rho(\text{Yellow–Blue})\equiv\rho(\text{Yellow})-\rho(\text{Blue})=-0.05\rho_{\text{rhod}}-0.36\rho_{\text{batho}}+0.41\rho_{\text{iso}}$; and (3) $\Delta\rho(\text{Red–Yellow})\equiv\rho(\text{Red})-\rho(\text{Yellow})=0.37\rho_{\text{rhod}}-0.37\rho_{\text{iso}}$, where ρ(Red), ρ(Blue), and ρ(Yellow) are the electron density maps derived from diffraction data that were collected from the crystal states in red light (635 nm), blue light (473 nm), and yellow light (560 nm), respectively. Roughly speaking, the structural differences between Rhod and Batho, between Batho and Iso, and between Rhod and Iso would be estimated from Δρ(Yellow–Blue), Δρ(Red–Blue), and Δρ(Red–Yellow), respectively. However, as the crystals used for diffraction measurements were not very large (approximately 0.2 mm × 0.2 mm × 0.2 mm), exposure to a high X-ray dose (approximately 3×10^{15} photons/mm^2) was required to obtain these difference maps with a reasonable signal-to-noise ratio.

To reduce the undesired effects of irreversible X-ray-induced damages, we employed the procedure used by Matsui *et al.*[24] Namely, three sets of partial diffraction data, which covered a small area of reciprocal space (equivalent to a 15° rotation), were collected in sequence under different illumination conditions—(I) red light, (II) blue light, and (III) red light—for derivation of Δρ(Red–Blue). Such measurements were repeated for different orientations of the crystal, and the data collected under illumination conditions I, II, and III were separately merged to provide three complete data sets (F_{I}, F_{II}, and F_{III}), from which two difference Fourier maps ($|F_{\text{II}}|-|F_{\text{I}}|$ and $|F_{\text{II}}|-|F_{\text{III}}|$) were calculated. If irreversible radiolysis of Asp80 and breakage of the Cys108-Cys186 disulfide bond did not occur significantly during the data collection of one partial data set, their effects would be concealed in a difference map derived from the second data set (F_{II}) and the merged data ($F_{\text{I+III}}$) of the first and third data sets.

Figure 4a shows the difference map Δρ(Red–Blue) that was derived from diffraction data collected under red-light illumination ($F_{\text{I+III}}$) and those collected under blue-light illumination (F_{II}). This difference map, which comes mainly from the structural difference between Rhod and Batho, exhibits complementary positive and negative

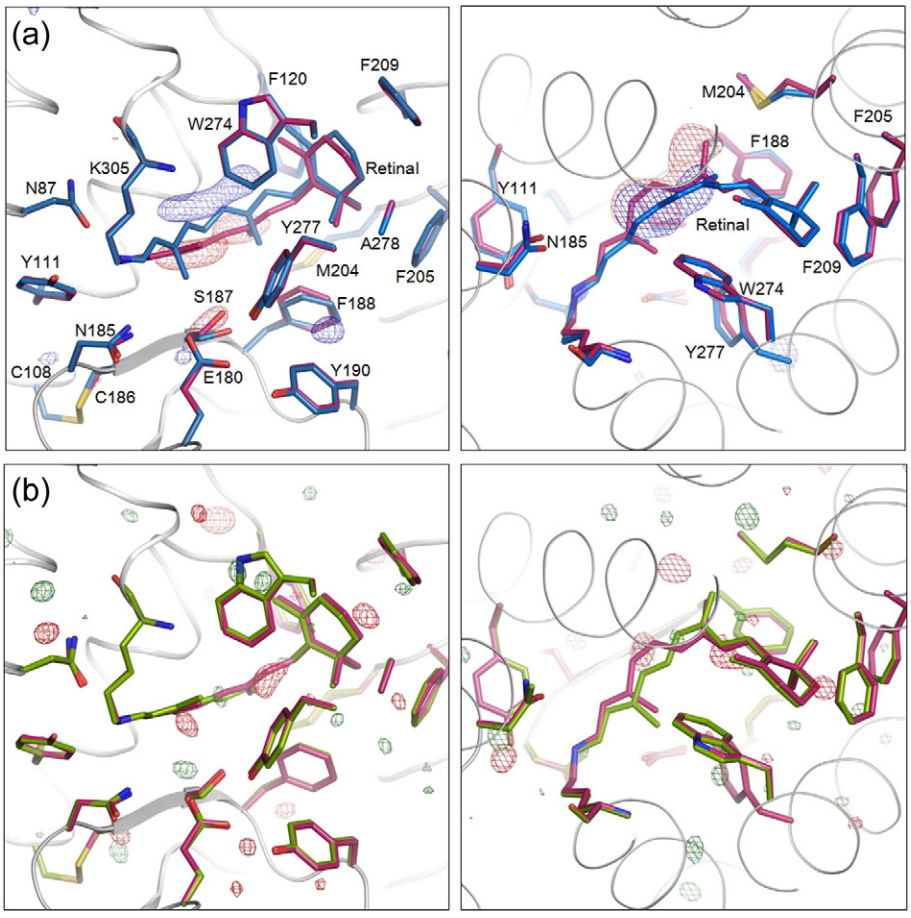

Fig. 4. Structural changes associated with interconversions among the three isomers (Rhod, Batho, and Iso). Using an X-ray flux rate of 9×10^{12} photons/mm^2/s, we collected three partial diffraction data sets ($|F_{\mathrm{I}}|$, $|F_{\mathrm{II}}|$, and $|F_{\mathrm{III}}|$) in the same range of oscillation but under different illumination conditions: (a) I, red light; II, blue light; III, red light; or (b) I, blue→red light; II, yellow light; III, blue→red light. Each diffraction image was taken with an oscillation angle of 1° and an exposure time of 2 s, and the illumination condition was alternated every 15 images. In total, 180 ($4\times15\times3$) images were taken from a single crystal, and the data taken under the same illumination were merged to obtain full data sets; that is, $|F_{(\mathrm{red})}|$ (←($|F_{\mathrm{I}}|+|F_{\mathrm{III}}|$)/2), $|F_{(\mathrm{blue})}|$, or $|F_{(\mathrm{yellow})}|$ (←$|F_{\mathrm{II}}|$). Here, $|F_{(\mathrm{blue})}|$, $|F_{(\mathrm{red})}|$, and $|F_{(\mathrm{yellow})}|$ are the structure factors derived from data sets collected under illumination with blue light at 473 nm (from a blue laser), with red light at 635 nm (from a red laser), and with green light at 570 nm (from a tungsten lamp passed through an interference filter), respectively. (a) $|F_{(\mathrm{blue})}|-|F_{(\mathrm{red})}|$ difference map and (b) $|F_{(\mathrm{red})}|-|F_{(\mathrm{yellow})}|$ difference map are contoured to 4.2σ (red, negative; blue and green, positive) and overlaid on the structural models of (a) Rhod and Batho and those of (b) Rhod and Iso. Carbon atoms in Rhod, Batho, and Iso are shown in magenta, blue, and green, respectively. Oxygen, nitrogen, and sulfur atoms are shown in red, blue, and green, respectively.

densities aligned parallel with the polyene chain of retinal. Another pair of positive and negative densities with smaller amplitudes is seen around the side chain of Ser187. Although the X-ray flux rate was not sufficiently low to prevent the formation of the orange species, the $F_{\mathrm{II}}-F_{\mathrm{I}}$ difference map coincided with the $F_{\mathrm{II}}-F_{\mathrm{III}}$ difference map. It is reasonable to interpret the complementary negative and positive densities seen in the central moiety of retinal (in the $|F_{\mathrm{I+III}}|-|F_{\mathrm{III}}|$ map) as originating from the structural change associated with the light-initiated interconversion (Batho→Rhod).

Figure 4b shows the difference map Δρ(Red–Yellow) derived from diffraction data collected under red-light illumination ($F_{\mathrm{I+III}}$) and those collected under yellow-light illumination (F_{II}). This difference map, which reflects the structural difference between Rhod and Iso, exhibited a negative density at the C11=C12 double bond of 11-*cis* retinal in Rhod and a positive peak at the C10 atom of 9-*cis* retinal in Iso. As these densities were very weak, it was suggested that the structural difference between Rhod and Iso was small.

Structures of Iso and Batho

Since Iso is the major isomeric component (approximately 98%) in the crystal illuminated with

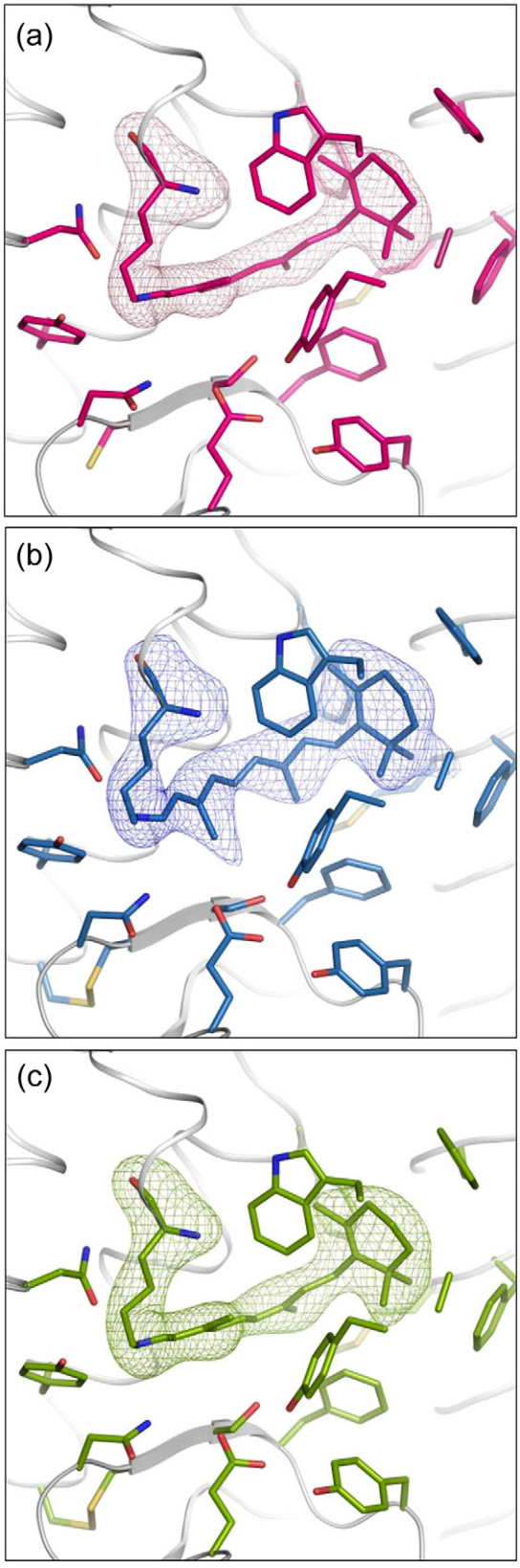

yellow light at 560 nm, the diffraction data collected under this illumination condition can be used to construct the structural model of Iso (Fig. 5c). The results suggested that 9-*cis* retinal in Iso took on a planar configuration. As expected from the difference map $\Delta\rho$(Red–Yellow), the overall shape of this isomer is quite similar to that of the 11-*cis* retinal in Rhod. Nonetheless, it was suggested that the interconversion from Rhod to Iso was accompanied by a small displacement of the central part (C8–C15) of the polyene chain, while the β-ionone ring and the Schiff base nitrogen scarcely moved.

The structural model of Batho was constructed using $\Delta\rho$(Red–Blue). Since the structural difference between Rhod and Iso is very small, the electron density map of Batho (ρ_{batho}) would be approximated by the following relationship: $\rho_{batho} \sim \rho(\text{Blue}) - \beta\Delta\rho(\text{Red–Blue})$, where β is a correction factor for the decrease in the content of the photochemically active protein during data collection. In the actual derivation of ρ_{batho}, we took into account the observation that a fraction ($f \sim 0.5$) of the protein was irreversibly damaged during exposure to an X-ray dose of 3×10^{15} photons/mm^2. Figure 5b shows the structural model of Batho that was constructed on the basis of this approximation. The result showed that the retinal in Batho took on a largely distorted all-trans configuration. Due to tight contact with the surrounding residues (five phenylalanine residues), the β-ionone ring scarcely moved upon the formation of Batho. Instead, the C13 methyl group pointed towards the extracellular side, pushing the side chain of Ser187 into the E-II loop. The C7=C8 double bond was twisted. The adjacent single and double bonds (C8–C9, C9=C10, C10–C11, and C11=C12) were also twisted so that the retinal polyene chain took on a curved structure around the indole ring of Trp274. Owing to the large twist of the retinal polyene chain, the Schiff base NH bond, which was directed towards Tyr111 in Rhod, was reorientated towards Asn87 in Batho.

Discussion

In this study, the electron density map of Batho was evaluated by a sophisticated method that was developed to reduce the possible effects of irreversible X-ray-induced damages. However, we have not yet succeeded in clarifying another type of X-ray damage (the reversible modification of retinal) that occurs at a very low dose of X-ray. In fact,

Fig. 5. Omit maps of the retinal–Lys305 chain and water molecules in (a) Rhod, (b) Batho, and (c) Iso contoured at 3.5σ and overlaid on the structural models of Rhod (magenta), Batho (pale), and Iso (lime). Oxygen, nitrogen, and sulfur atoms are shown in red, blue, and green, respectively.

model building of Batho was performed on the assumption that the shape of retinal did not significantly alter upon X-ray absorption. A possible influence of this assumption should not be underestimated because it has been recently reported that the 13-*cis* retinal in the M state of bacteriorhodopsin is converted partly into a retro form with an all-trans configuration by a low dose of X-ray ($<2\times10^{15}$ photons/mm^2).[28] If this scenario is applied to squid rhodopsin, it may be argued that the retinal in Batho is modified in such a manner that the mechanical stress in the retinal-binding pocket is reduced (i.e., the X-ray product of Batho may be rather similar to that of Rhod). In such a case, the retinal in Batho would be expected to be actually more distorted than that shown in Fig. 5b. It should be noted that what we can determine is the average structure of Batho and its X-ray product, which are in dynamic equilibrium during the X-ray exposure. Although there remains ambiguity in evaluating the extent of retinal distortion in Batho, the essence of the structural difference between Batho and Rhod can be discussed safely on the basis of the difference map shown in Fig. 4a. This difference map strongly suggests that the two terminal ends of retinal scarcely move upon the formation of Batho, while the central part of the retinal polyene chain moves towards the cytoplasmic side. This feature is explained well by a structural model of Batho in which the all-*trans* retinal has a right-handed screwed configuration. This configuration of retinal is consistent with the CD spectrum of Batho, which has a negative band at 535 nm.[22]

When the structural models of the three isomers (Rhod, Batho, and Iso) are compared, it is suggested that the steric interactions between retinal and the surrounding residues determine the excited-state dynamics. In Rhod or Iso, the polyene chain of retinal is clamped between helix III and a β-strand in the E-II loop so that its planar plane is orientated perpendicular with the membrane normal. In contrast, the retinal in Batho is largely distorted. Firstly, the C13 methyl directs towards a β-strand in the E-II loop, pushing the side chain of Ser187. The C9 methyl also directs towards the E-II loop, pushing Phe188. The steric repulsions between these methyl groups and the residues in the E-II loop force the central moiety of the polyene chain to move towards the cytoplasmic side. Since the ionone ring and the Schiff base scarcely move in the formation process of Batho, the polyene chain is largely twisted around the C7=C8, C9=C10, and C11=C12 bonds. Owing to this twisting, the Schiff base NH bond reorientates towards Asn87. This reorientation is accompanied by an alteration in the hydrogen-bonding network near the Schiff base. For example, a water molecule (Wat508), which is hydrogen bonded to the main-chain carbonyl of Lys305 in Rhod, was suggested to move towards the Schiff base upon the formation of Batho. This may evoke a rearrangement of the hydrogen-bonding network extending from the active site to the cytoplasmic surface.[17] It is also possible that a few water molecules, which are not clearly visible in the electron density map, diffuse into a large cavity that is created between the twisted polyene chain and the wall of the retinal-binding pocket. These possibilities warrant further investigation because a previous Fourier transform infrared spectroscopy study showed that more than eight water molecules change their vibration frequencies upon the formation of Batho.[9]

Figure 6 compares the structural change in the primary photoreaction of squid rhodopsin to that of

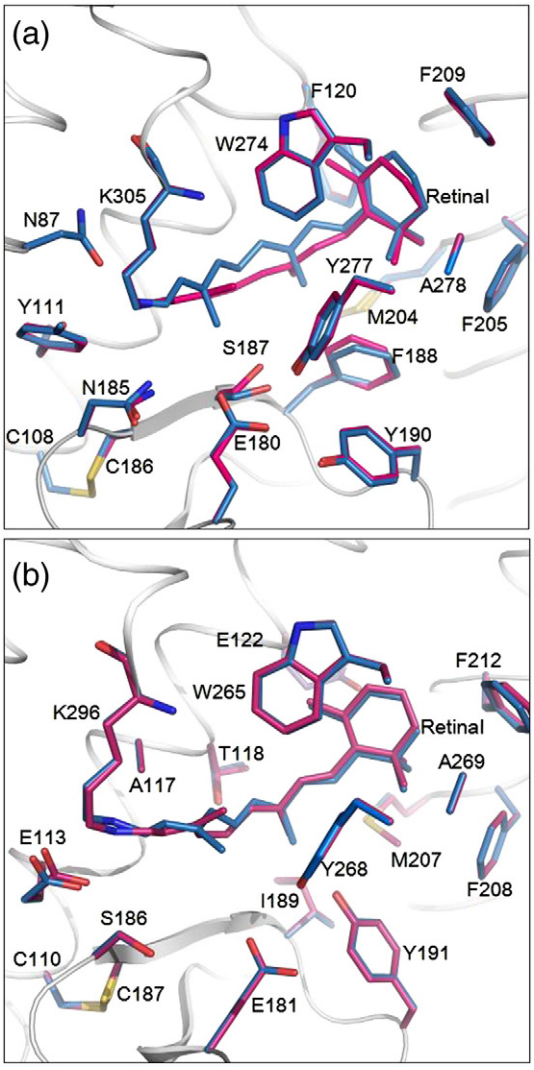

Fig. 6. Structural changes in the primary photoreaction in (a) squid rhodopsin and (b) bovine rhodopsin. Carbon atoms are shown in magenta (Rhod) or pale (Batho); oxygen, nitrogen, and sulfur atoms are shown in red, blue, and green, respectively.

bovine rhodopsin. Although a large rotation (approximately 90°) of the central part of the retinal polyene chain is observed in squid rhodopsin, this reorientation is not clearly seen in bovine rhodopsin.[16,19] This difference comes mainly from a large difference in the retinal configuration in Rhod for squid and bovine rhodopsins. Interestingly, there is little difference in the retinal configuration in Batho for squid and bovine rhodopsins. It has been reported that a similar energy (35 kcal/mol) is stored in Batho for vertebrate and invertebrate rhodopsins.[12,13,29,30] This similarity can be understood by supposing that the configuration of the retinal in Batho is conserved among these rhodopsins. However, this does not necessarily mean that excited-state dynamics are also similar for these rhodopsins. It has been demonstrated that the speed of cis–trans isomerization is much more slower in squid rhodopsin than in bovine rhodopsin.[10,11] This difference is probably related to variations in the local structure of the retinal-binding pocket. For activation of bovine rhodopsin, a steric interaction between the C9 methyl group and Thr118 in helix III has been reported to play an important role.[31,32] This steric interaction is less significant in squid rhodopsin, where the C9 methyl group associates with a smaller residue (Gly116). It is likely that the negative barrier to cis-to-trans photoisomerization is less steep in squid rhodopsin than in bovine rhodopsin. Hence, it is not surprising to note that the spectral data of squid rhodopsin (Fig. 1) are explained well by the common excited-state model, while this model was reported to be inadequate for describing the excited-state dynamics of bovine rhodopsin.[33] Our observation is consistent with the previous prediction that "torsion potential," which originates from the protein environment, drives the efficient isomerization of retinal.[34]

The structures of Iso and Rhod showed that there was no large difference in the overall structures of retinal between these isomeric states. Conversely, the spectral data shown in Fig. 1 suggested that the quantum efficiency of Rhod-to-Batho conversion was approximately 60 times higher than that of Iso-to-Batho conversion. One possible reason for this difference is the presence of a negatively charged residue (Glu180) near the C11=C12 double bond (Fig. 5). It has been predicted that, upon torsional distortion around the cis linkage, a large shift of negative charge is induced out of this region.[35] The result from the present study suggests that this charge reorganization, which helps drive photoisomerization by preferential stabilization of the 11-orthogonal conformation, is enhanced by the presence of a negative charge.

The photoisomerization mechanism of rhodopsin has been discussed from a theoretical viewpoint. Previous models, such as the bicycle-pedal model[36] and the hula-twist model,[37] suggested that, upon photoisomerization, rotation around the C11=C12 bond propagated to neighboring double and/or single bonds. Our model for Batho shows that, besides the C11=C12 bond, the C7=C8 double bond undergoes a large rotation in a bicycle-pedal fashion; in addition, every bond between these double bonds also twists to form a curved structure. Therefore, each of the previous theoretical predictions has partially described a complicated rotational motion in the experimental model of squid Batho.

Materials and Methods

Protein purification and crystallization

All manipulations were performed in dim red light (>640 nm). Squid (*Todarodes pacificus*) rhodopsin contains 448 amino acids with a molecular mass of 50 kDa. C-terminally truncated squid rhodopsin was crystallized as described previously.[38] Briefly, the extension in the C-terminal region was removed by cleaving a peptide bond at Glu373 (or Glu358) with V8 protease. The truncated rhodopsin was extracted selectively from microvillar membranes with octylglucoside in the presence of zinc acetate and was crystallized into the hexagonal $P6_2$ crystal.

Measurements of absorption spectra

The absorption spectra of a frozen crystal of squid rhodopsin were measured with a microspectrophotometer in which monochromatic light from a double monochromator (UV350A; Shimadzu) was focused on a small area of the crystal, and the intensity of transmitted light was measured with a photomultiplier tube, as described previously.[39] A frozen crystal was mounted onto a goniometer head attached to the microspectrometer, and the temperature was controlled in a flow of cold nitrogen gas from a cryostreamer (CC-12; Oxford Cryosystems). For absorption measurement of Rhod of squid rhodopsin, crystal mounting was operated in dim red light. For investigation of the isomeric composition in a frozen crystal after irradiation at various wavelengths, the frozen crystal was irradiated with monochromatic light from a blue laser ($\lambda = 473$ nm, 2 mW/mm^2) for 3 min and subsequently irradiated with monochromatic light that was obtained by passing white light from a tungsten lamp (150 W) through an interference filter (Toshiba) with a full width at half maximum of 10 nm.

Data collection

A single crystal was transferred into a solution containing 30 mM octylglucoside, 3.2 M ammonium sulfate, 40 mM 4-morpholineethanesulfonic acid (pH 6.4), and 20% sucrose. After a 10-min soak, the crystal was flash-frozen in liquid propane held at its melting temperature and stored in liquid nitrogen. X-ray diffraction measurements were performed at SPring-8 BL26B2, SPring-8 BL38B1, and

Table 1. Data collection and refinement statistics

	Batho	Iso-1	Iso-2
Data collection			
Space group	$P6_2$	$P6_2$	$P6_2$
Cell dimensions			
a, *b*, *c* (Å)	122.36, 122.36, 158.22	122.52, 122.52, 158.48	122.59, 122.59, 158.02
α, β, γ (°)	90, 90, 120	90, 90, 120	90, 90, 120
Twin fraction (%)	16	42	23
Resolution (Å)	88.04–2.80 (2.95–2.80)	61.26–2.70 (2.85–2.70)	61.28–2.80 (2.95–2.80)
R_{sym} or R_{merge}	0.078 (0.529)	0.086 (0.527)	0.087 (0.483)
$I/\sigma I$	11.2 (2.0)	10.9 (2.6)	10.3 (2.3)
Completeness (%)	95.5 (95.0)	99.7 (100)	99.6 (98.6)
Redundancy	3.3 (2.8)	3.7 (3.7)	3.5 (3.2)
Refinement			
Resolution (Å)	15.0–2.8	15–2.7	15.0–2.8
Number of reflections	22,229	33,666	32,922
R_{work}/R_{free}	0.295/0.345	0.180/0.200	0.249/0.267
Protein atoms	5542	5542	5839
Number of lipid molecules	2	3	8
Number of water molecules	59	59	59
R.m.s.d.			
Bond lengths (Å)	0.021	0.016	0.015
Bond angles (°)	1.7	1.6	1.5

Photon Factory AR-NW14A, where a frozen crystal kept at 100 K was exposed to a monochromatic X-ray beam at a wavelength of 1.0 Å. Indexing and integration of diffraction spots were carried out with MOSFLM 7.04.[40] Scaling of data was carried out using SCALA[41] in the CCP4 program suites.[42] All figures were generated using PyMOL.[43]

To investigate structural differences between Rhod and Batho, we adopted the previous procedure that we performed for the K intermediate of bacteriorhodopsin,[24] with slight modifications. Three sequential partial data with alternative illumination of red light (λ = 635 nm, 0.9 mW/mm^2), blue light (λ = 473 nm, 2 mW/mm^2), and red light (λ = 635 nm, 0.9 mW/mm^2) were collected with a flux of X-rays (3×10^{15} photons/mm^2) in sequence under the following illumination conditions: (I) red light, (II) blue light, and (III) red light. Such measurements were repeated every 15° up to a total of 180 images, and the data collected under illumination conditions I, II, and III were merged separately to provide three complete data sets (F_I, F_{II}, and F_{III}). A difference map derived from the second data set (F_{II}) and from the merged data (F_{I+III}) of the first and third data sets was used to investigate the structural difference between Batho and Rhod.

Structure refinement

Structure refinement was performed with CNS 1.2[44,45] and XtalView 4.1.[46] Diffraction data from the hexagonal crystal were fitted well by unit cell parameters described in Table 1.

Model building was performed by the molecular replacement method, with the structure of squid rhodopsin (Protein Data Bank ID: 2Z73) as initial search model. Diffraction intensities from a partially twinned crystal (twinning fraction ~0.16) were detwinned by CCP4, and the resulting $I_{detwin}(hkl)$ intensities were used to build a structural model at 2.8 Å resolution.

Accession number

Crystallographic coordinates of squid Batho and Iso have been deposited at the Protein Data Bank with accession codes 3AYM and 3AYN, respectively.

Acknowledgements

We wish to express our gratitude to Drs. S. Adachi, N. Shimidzu and K. Baba for helping with data collection at beamlines BL26B2 and BL38B1 of SPring-8 and AR-NW14A of Photon Factory. This work was supported by a grant-in-aid from the Ministry of Education, Science, and Culture of Japan.

References

1. Hubbard, R. & St. George, R. C. (1958). The rhodopsin system of the squid. *J. Gen. Physiol.* **41**, 501–528.
2. Yarfitz, S. & Hurley, J. B. (1994). Transduction mechanisms of vertebrate and invertebrate photoreceptors. *J. Biol. Chem.* **269**, 14329.
3. Yoshizawa, T. & Wald, G. (1963). Pre-lumirhodopsin and the bleaching of visual pigments. *Nature*, **197**, 1279–1286.
4. Yoshizawa, T. & Wald, G. (1964). Transformations of squid rhodopsin at low temperatures. *Nature*, **201**, 340–345.
5. Palings, I., van den Berg, E. M., Lugtenburg, J. & Mathies, R. A. (1989). Complete assignment of the hydrogen out-of-plane wagging vibrations of bathorhodopsin: chromophore structure and energy storage in the primary photoproduct of vision. *Biochemistry*, **28**, 1498–1507.

6. Smith, S. O., Courtin, J., de Groot, H., Gebhard, R. & Lugtenburg, J. (1991). ^{13}C magic-angle spinning NMR studies of bathorhodopsin, the primary photoproduct of rhodopsin. *Biochemistry*, **30**, 7409–7415.
7. Bagley, K. A., Balogh-Nair, V., Croteau, A. A., Dollinger, G., Ebrey, T. G., Eisenstein, L. *et al.* (1985). Fourier-transform infrared difference spectroscopy of rhodopsin and its photoproducts at low temperature. *Biochemistry*, **22**, 6055–6071.
8. Sulkes, M., Lewis, A. & Marcus, M. A. (1978). Resonance Raman spectroscopy of squid and bovine visual pigments: the primary photochemistry in visual transduction. *Biochemistry*, **17**, 4712–4722.
9. Ota, T., Furutani, Y., Terakita, A., Shichida, Y. & Kandori, H. (2006). Structural changes in the Schiff base region of squid rhodopsin upon photoisomerization studied by low-temperature FTIR spectroscopy. *Biochemistry*, **45**, 2845–2851.
10. Schoenlein, R. W., Peteanu, L. A., Mathies, R. A. & Shank, C. V. (1991). The first step in vision: femtosecond isomerization of rhodopsin. *Science*, **254**, 412–415.
11. Matuoka, S., Shichida, Y. & Yoshizawa, T. (1984). Formation of hypsorhodopsin at room temperature by picosecond green pulse. *Biochim. Biophys. Acta*, **765**, 38–42.
12. Dartnall, H. J. (1968). The photosensitivities of visual pigments in the presence of hydroxylamine. *Vision Res.* **8**, 339–358.
13. Suzuki, T. & Callender, R. H. (1981). Primary photochemistry and photoisomerization of retinal at 77 degrees K in cattle and squid rhodopsins. *Biophys. J.* **34**, 261–270.
14. Becker, R. S. & Freedman, K. (1985). A comprehensive investigation of the mechanism and photophysics of isomerization of a protonated and unprotonated Schiff base of 11-*cis*-retinal. *J. Am. Chem. Soc.* **107**, 1477–1485.
15. Palczewski, K., Kumasaka, T., Hori, T., Behnke, C. A., Motoshima, H., Fox, B. A. *et al.* (2000). Crystal structure of rhodopsin: a G protein-coupled receptor. *Science*, **289**, 739–745.
16. Okada, T., Sugihara, M., Bondar, A. N., Elstner, M., Entel, P. & Buss, V. (2004). The retinal conformation and its environment in rhodopsin in light of a new 2.2 Å crystal structure. *J. Mol. Biol.* **342**, 571–583.
17. Murakami, M. & Kouyama, T. (2008). Crystal structure of squid rhodopsin. *Nature*, **453**, 363–367.
18. Yan, E. C., Kazmi, M. A., Ganim, Z., Hou, J. M., Pan, D., Chang, B. S. *et al.* (2003). Retinal counterion switch in the photoactivation of the G protein-coupled receptor rhodopsin. *Proc. Natl Acad. Sci. USA*, **100**, 9262–9267.
19. Nakamichi, H. & Okada, T. (2006). Crystallographic analysis of primary visual photochemistry. *Angew. Chem. Int. Ed. Engl.* **45**, 4270–4273.
20. Sugihara, M., Hufen, J. & Buss, V. (2006). Origin and consequences of steric strain in the rhodopsin binding pocket. *Biochemistry*, **24**, 801–810.
21. Nakamichi, H., Buss, V. & Okada, T. (2007). Photoisomerization mechanism of rhodopsin and 9-*cis*-rhodopsin revealed by X-ray crystallography. *Biophys. J.* **92**, 106–108.
22. Shichida, Y., Tokunaga, F. & Yoshizawa, T. (1978). Circular dichroism of squid rhodopsin and its intermediates. *Biochim. Biophys. Acta*, **504**, 413–430.
23. Maeda, A., Ogurusu, T., Shichida, Y., Tokunaga, F. & Yoshizawa, T. (1978). Formation of a 7-*cis* retinal pigment by irradiating cattle rhodopsin at low temperatures. *FEBS Lett.* **92**, 77–80.
24. Matsui, Y., Sakai, K., Murakami, M., Shiro, Y., Adachi, S., Okumura, H. & Kouyama, T. (2002). Specific damage induced by X-ray radiation and structural changes in the primary photoreaction of bacteriorhodopsin. *J. Mol. Biol.* **324**, 469–481.
25. Okumura, H., Murakami, M. & Kouyama, T. (2005). Crystal structures of acid blue and alkaline purple forms of bacteriorhodopsin. *J. Mol. Biol.* **351**, 481–495.
26. Takeda, K., Matsui, Y., Kamiya, N., Adachi, S., Okumura, H. & Kouyama, T. (2004). Crystal structure of the M intermediate of bacteriorhodopsin: allosteric structural changes mediated by sliding movement of a transmembrane helix. *J. Mol. Biol.* **341**, 1023–1037.
27. Weik, M., Ravelli, R. B., Kryger, G., McSweeney, S., Raves, M. L., Harel, M. *et al.* (2000). Specific chemical and structural damage to proteins produced by synchrotron radiation. *Proc. Natl Acad. Sci. USA*, **97**, 623–628.
28. Yamamoto, M., Hayakawa, N., Murakami, M. & Kouyama, T. (2009). Crystal structures of different substates of bacteriorhodopsin's M intermediate at various pH levels. *J. Mol. Biol.* **393**, 559–573.
29. Cooper, A. (1979). Energy uptake in the first step of visual excitation. *Nature*, **282**, 531–533.
30. Nishioku, Y., Nakagawa, M., Tsuda, M. & Terazima, M. (2002). Energetics and volume changes of the intermediates in the photolysis of octopus rhodopsin at a physiological temperature. *Biophys. J.* **83**, 1136–1146.
31. Ganter, U. M., Schmid, E. D., Perez-Sala, D., Rando, R. R. & Siebert, F. (1989). Removal of the 9-methyl group of retinal inhibits signal transduction in the visual process. A Fourier transform infrared and biochemical investigation. *Biochemistry*, **28**, 5954–5962.
32. Han, M., Groesbeek, M., Smith, S. O. & Sakmar, T. P. (1998). Role of the C9 methyl group in rhodopsin activation: characterization of mutant opsins with the artificial chromophore 11-*cis*-9-demethylretinal. *Biochemistry*, **37**, 538–545.
33. Rosenfeld, T., Honig, B., Ottolenghi, M., Hurley, J. & Ebrey, T. G. (1977). Cis–trans isomerization in the photochemistry of vision. *Pure Appl. Chem.* **49**, 341–351.
34. Kakitani, T. & Kakitani, H. (1975). Molecular mechanism for the initial process of visual excitation: I. Model of photoisomerization in rhodopsin and its theoretical basis by a quantum mechanical calculation of adiabatic potential. *J. Phys. Soc. Jpn.* **38**, 1455–1463.
35. Birge, R. R., Einterz, C. M., Knapp, H. M. & Murray, L. P. (1988). The nature of the primary photochemical events in rhodopsin and isorhodopsin. *Biophys. J.* **53**, 367–385.
36. Warshel, A. (1976). Bicycle-pedal model for the first step in the vision process. *Nature*, **260**, 679–683.
37. Liu, R. S. & Asato, A. E. (1985). The primary process of vision and the structure of bathorhodopsin: a mechanism for photoisomerization of polyenes. *Proc. Natl Acad. Sci. USA*, **82**, 259–263.
38. Murakami, M., Kitahara, R., Gotoh, T. & Kouyama, T. (2007). Crystallization and crystal properties of squid rhodopsin. *Acta Crystallogr., Sect F*, **63**, 475–479.
39. Sakai, K., Matsui, Y., Kouyama, T., Shiro, Y. & Adachi, S. (2002). Optical monitoring of freeze-trapped

reaction intermediates in protein crystals: a microspectrophotometer for cryogenic protein crystallography. *J. Appl. Crystallogr.* **35**, 270–273.
40. Leslie, A. G. W. (1992). Recent changes to the MOSFLM package for processing film and image plate data. *Jt. CCP4+ESF-EAMCB Newsl. Protein Crystallogr.* **26**.
41. Evans, P. (2006). Scaling and assessment of data quality. *Acta Crystallogr., Sect. D: Biol. Crystallogr.* **62**, 72–82.
42. Collaborative Computational Project, Number 4. (1994). The CCP4 Suite: programs for protein crystallography. *Acta Crystallogr., Sect. D: Biol. Crystallogr.* **50**, 760–763.
43. Baker, N. A., Sept, D., Joseph, S., Holst, M. J. & McCammon, J. A. (2001). Electrostatics of nanosystems: application to microtubules and the ribosome. *Proc. Natl Acad. Sci. USA*, **98**, 10037–10041.
44. Brünger, A. T., Adams, P. D., Clore, G. M., Gros, P., Grosse-Kunstleve, R. W., Jiang, J. S. *et al.* (1998). Crystallography & NMR System (CNS): a new software suite for macromolecular structure determination. *Acta Crystallogr., Sect. D: Biol. Crystallogr.* **54**, 905–921.
45. Brünger, A. T. (2007). Version 1.2 of the Crystallography and NMR System. *Nat. Protoc.* **2**, 2728–2733.
46. McRee, D. E. (1993). *Practical Protein Crystallography.* Academic Press, San Diego, CA.